

TOPICAL REVIEW

Hydrodynamic effects in proteins

Piotr Szymczak¹ and Marek Cieplak²¹ Institute of Theoretical Physics, Faculty of Physics, University of Warsaw, Hoża 69, 00-681 Warsaw, Poland² Institute of Physics, Polish Academy of Sciences, Aleja Lotników 32/46, 02-668 Warsaw, PolandE-mail: piotr.szymczak@fuw.edu.pl

Received 26 July 2010, in final form 16 November 2010

Published 16 December 2010

Online at stacks.iop.org/JPhysCM/23/033102**Abstract**

Experimental and numerical results pertaining to flow-induced effects in proteins are reviewed. Special emphasis is placed on shear-induced unfolding and on the role of solvent mediated hydrodynamic interactions in the conformational transitions in proteins.

(Some figures in this article are in colour only in the electronic version)

Contents

1. Introduction	1
2. Proteins in the flow: experimental results	1
3. Computational techniques	3
3.1. All-atom protein simulations with an explicit solvent	3
3.2. Coarse-grained protein models with an implicit solvent	3
3.3. Langevin dynamics	3
3.4. Overdamped limit and Brownian dynamics	4
3.5. Inclusion of flow and hydrodynamic interactions	4
3.6. Mesoscopic solvent models	6
3.7. Other computational approaches	6
4. Numerical studies of flow-induced conformational changes in proteins	6
5. Flow-induced tension along the chain	8
6. Effects of hydrodynamic interactions on protein unfolding	9
7. Summary	10
Acknowledgments	11
Appendix. Estimate of the critical strain rate	11
References	11

the impact of larger-scale, hydrodynamic processes on protein dynamics is considered less frequently, even though strong fluid flows may unfold the protein molecule as effectively as the mechanical force in atomic force microscopy (AFM) experiments. In fact, as we elucidate below, hydrodynamic forces provide a more versatile tool for probing protein structure, since they induce highly non-uniform tension along the protein, probing different bond groups with different intensities. As is to be expected, Nature has found a way to exploit the sensitivity of proteins to hydrodynamic forces in a variety of regulatory processes, the best known of which is hemostasis, where hydrodynamic shear was found to activate binding of the plasma protein von Willebrand factor (vWf) to the platelet receptor glycoprotein Ib (GpIb). Below, we briefly review the most important experimental and theoretical investigations of flow-related effects in proteins. The review is supplemented with a short description of relevant numerical techniques. We outline the latest numerical results on flow-induced conformational changes in proteins and on the role of hydrodynamic interactions (HI) in such changes. We also discuss the influence of HI on protein folding and on the distribution of tension along a string of beads submitted to a flow.

1. Introduction

Water constitutes a natural environment for protein molecules: it stabilizes their native structures, influences their enzymatic activity and is critical in phenomena such as molecular recognition and protein–protein interactions [1, 2]. However,

2. Proteins in the flow: experimental results

Almost all of the reported experiments on flow effects on protein structures have been performed using shear flow. There are two reasons why experiments with shear flow are particularly attractive. The first is the ease with which this

type of flow can be generated. In fact a nonzero shear component appears whenever a fluid flows along a surface, including different kinds of capillary flows. The second reason is that shear flow has a significant effect on the dynamics of suspended biopolymers even in the absence of any tethering.

As noted by several authors [3, 4], the experimental results on shear flow unfolding are rather ambiguous: while some studies claim that changes in the protein structure take place at shear rates as low as $\dot{\gamma} = 10 \text{ s}^{-1}$ [5, 6, 4] other researchers found no indication of shear mediated unfolding even at $\dot{\gamma} = 10^5 \text{ s}^{-1}$ [7–10, 3, 11]. Apparently, the situation here is rather complex, with factors like the presence of liquid–air interface or interaction with a solid surface playing an important role [10]. Also, some effects of the shear are apparently of a cumulative nature and should be described in terms of the strain history $\gamma = \tau_s \dot{\gamma}$ (where τ_s is the total time during which the sample was exposed to the shear). Jaspe and Hagen [3] gave a simple theoretical estimate of the threshold shear rate capable of unfolding a typical protein molecule (which is reproduced in the appendix). In terms of the dimensionless Weissenberg number, $Wi = \dot{\gamma} \tau_r$, this threshold corresponds to $Wi \sim 10^3$. Here τ_r is the longest relaxation time of an unperturbed molecule.

The longer the molecule and the more extended its conformation, the larger effect shear forces have on its stability. This is the reason why it is, in general, much easier to use hydrodynamic shear to induce conformational changes in long (μm scale) DNA chains than in much shorter (nm scale) protein molecules. However, long, multi-unit proteins are more susceptible to shear. A well-studied example is von Willebrand factor (vWf), a huge multi-unit protein found in blood plasma which can reach extensions of up to $100 \mu\text{m}$ [12]. Von Willebrand factor plays a central role in a process of platelet adhesion to the sites of vascular injury and is thus a key component for maintenance of normal hemostasis.

The existence of shear-induced conformational transitions in this system is well documented experimentally. In fact, shear field impacts upon vWf structure at a variety of levels. First of all, shear flow induces a change in the quaternary structure of the whole multi-unit chain, from a compact globular state to the elongated fiber-like conformation [13–16]. This structural transition takes place at $\dot{\gamma} = 5 \times 10^3 \text{ s}^{-1}$, which is more than two orders of magnitude higher than the values reported for DNA of the same length. This is probably due to the significant role of attractive forces of hydrophobic origin between the vWf units. Importantly, the structural transition of vWf multimers into elongated fibers dramatically increases its adhesion rate to the fibrillar collagen of the vessel walls [15]. High shear conditions were also reported to trigger novel disulfide bond formation in the protein [17], promoting self-assembly of vWf into a network of fibers.

Additionally, the shear flow activates the binding of platelets to vWf by inducing a structural transition in the A1 domain of the vWf multimer to an intermediate conformation that can bind the platelet receptor GpIb α [18–20]. Interestingly, GpIb α itself has also been shown to undergo flow-induced conformational changes [21, 22].

The fact that hydrodynamic forces induce conformational transitions in vWf may provide a basis for a self-regulatory

repair mechanism of blood vessel walls: in the case of damage, the shear stresses increase, which induces transitions of the vWf structure that seem to be necessary for the initiation of platelet adhesion [23, 24].

There is yet another shear-induced mechanism in hemostasis that has attracted considerable interest [25–27]: the cleavage of ultra-large vWf into smaller multimers. The single-molecule laser-tweezer experiments by Zhang *et al* [27] have shown that mechanical forces in the range experienced by vWf due to flow in the vasculature can unfold the A2 domain of vWf which subsequently enables cleavage by the metalloprotease ADAMTS13. Thus the A2 domain plays the role of a shear bolt for the vWf structure [27]. In engineering, a shear bolt is designed to break above a certain threshold force to protect other parts of a machine from accidental damage, and here unfolding of the A2 domain takes place to allow for ADAMTS13 cleavage, which results in down-regulation of hemostatic activity. Interestingly, Zhang *et al* [27] suggest that typical shear forces in the vasculature might not be sufficiently high to effectively unfold A2 and that the unfolding might take place due to the purely elongational flow. Elongation may be induced by the process of vasoconstriction that causes the vessel to constrict to a smaller radius during an injury. Elongational flow in the vasculature can induce unfolding forces in vWf which are larger by one to two orders of magnitude from those experienced in a pure shear flow [28] (see also the discussion of elongational flow in sections 4 and 5).

Other, relatively large, μm -scale protein structures that are affected by hydrodynamic shear are amyloid fibrils. Studies on β -lactoglobulin fibrils [29, 30] show that shear affects both the formation of the fibril structures and their breakup. In particular, it has been hypothesized that the shear flow degradation of lactoglobulin fibers in the blood stream might provide a mechanism for amyloid disease propagation. In similar studies, Bhak *et al* [31] and Dunstan *et al* [32] have shown that shear forces dramatically increase the rate of fibril formation. Lokszejn and Dzwolak in [33] studied insulin fibrillation and hypothesized that hydrodynamic forces play a key role in that process, promoting insulin aggregation and subsequent formation of chiral amyloid superstructures. Finally, Lee *et al* [34] studied amyloid formation in a microfluidic device, analyzing the influence of the flow rate on the kinetics of the process.

Another possible way to increase the shear-induced forces is to use a solvent with a larger viscosity than water, as is the case in the study by van der Veen *et al* [35] on α -amylase deactivation in concentrated starch solution. Due to the very high viscosity of the medium, relatively large shear stresses of about $3 \times 10^4 \text{ Pa}$ were reached, which have partially deactivated the enzyme by deforming its tertiary structure. These results are consistent with the study of Ashton *et al* [4] who have reported that the shear-induced conformational changes in lysosomes are significantly larger with a glycerol as a solvent than water.

In the context of regulatory mechanisms in which hydrodynamic shear forces seem to be involved one needs to mention also the activation of ion channels in both

endothelial [36] and epithelial [37–40] cells. In particular, the physiological relevance of shear stress as an adequate stimulus for ENaC (epithelial Na⁺ channel) activation has been demonstrated experimentally by exposing the ion channel expressing membranes to a flow of different magnitude while simultaneously monitoring the Na⁺ absorption [37, 39]. Furthermore, it has been observed that if ENaCs are first chemically activated and subsequently exposed to shear forces, then the effect of shear is much weaker. This indicates that hydrodynamic shear may activate ENaCs by altering gating properties and thus increasing the open probability of the channels. The sensitivity of epithelial ion channels to the shear force has a physiological basis, since these channels usually function in Na⁺ adsorbing epithelia, such as kidney or lung, where there is a fluid flow present—urinary fluid in the kidney tubules and airflow in lungs.

In summary, most of the flow denaturation experiments of proteins have been carried out on a bulk collection of molecules, usually subject to shearing forces. Single-molecule studies are still scarce and limited mostly to large micrometer-size structures, like ultralong multi-unit vWf molecules or amyloid fibrils, where mostly quaternary structural changes are induced by the presence of the flow. It is expected that the development of new experimental techniques will greatly increase the possibilities to study these systems, and provide direct evidence for flow-induced changes to the tertiary structure of single protein molecules.

3. Computational techniques

Before proceeding with the discussion of the numerical results on the flow-induced effects in proteins, we briefly review the computational methods used in these studies.

3.1. All-atom protein simulations with an explicit solvent

A most detailed description of the protein in a hydrodynamic flow is obtained by modeling the system at atomic resolution. A number of such studies have been reported recently: Wang *et al* [41] analyzed unfolding of tethered ubiquitin in a uniform flow whereas Lou *et al* [21] and Chen *et al* [22] analyzed the influence of the flow on conformational changes in glycoprotein Ib. In the former study, the flow in the system was induced by translating two frozen water surfaces in the given direction, and letting their atoms interact with the rest of the system. In the latter case, the flow was induced by the application of a constant force to all the water molecules, while simultaneously coupling them to a Langevin thermostat to prevent overheating.

The main deficiency of the all-atom approaches is their high computational cost which prevents them from being used to compute ensemble properties requiring the analysis of many pathways and necessitates the use of extremely fast flows, which allow observation of the conformational changes over the short time scales accessible in such simulations.

For example, in [21, 22] flow velocities of 50 m s⁻¹ were used, which is about two orders of magnitude faster than blood flow velocities in large arteries and even as much as

eight orders of magnitude faster than velocities in small blood vessels and near vessel walls. The total simulation time for each trajectory was 20 ns. In [41] the flow velocities were even higher (180 m s⁻¹) and the total simulation times shorter (hundreds of ps to ns). This is particularly relevant, since at short time scales and high flow rates the fluid inertia effects become important (see the discussion in section 3.3). This may lead to a qualitatively different physical phenomenon from those at lower flow rates and it is not clear whether the obtained results indeed correspond to the flow effects in a real system. In fact, Wang *et al* [41] have indeed observed strong flow inertia-related effects in their studies.

3.2. Coarse-grained protein models with an implicit solvent

Because of the high computational cost of atomistic simulations and their inability to consider time scales relevant to many flow-induced conformational changes, a large number of simulation studies resort to coarse-grained protein models. In these models, each residue is represented as a number of beads that interact via effective force-fields [42–45]. In the simplest version, there is just a single bead per residue (usually centered on the position of the C^α atom), whereas more complex models involve additional beads representing side groups of the amino acids.

Despite their simplicity, coarse-grained models capture many features of folding and unfolding of proteins observed experimentally. In particular, a detailed comparison between the experimental data on the mechanical resistance of proteins and the prediction of coarse-grained models [46, 47] shows a very good correlation between the two.

A particularly widely used class of coarse-grained models is the group of structure-based, Go-type models, in which an effective potential of interaction between amino acids is constructed in such a way as to guarantee that the known native structure of the protein corresponds to the global energy minimum. Hydrodynamic effects in proteins have been studied using different versions of these models, e.g. in [48–54].

On the other hand, Lemak *et al* [55, 56] have studied flow effects in a minimal model of an α -helix bundle and β -barrel originally introduced by Honeycutt and Thirumalai [57]. The key components of the potential energy in these models include the bond angle potential, a heterogeneous long-range Lennard-Jones potential reflecting the three different types of residues, hydrophobic, hydrophilic, and neutral, and a torsional-angle potential that effectively prefers a local α -helix or β -sheet conformation. An analogous model was used by Baumketner and Hiwatari [58] in their studies of hydrodynamic interaction effects in protein folding.

In the coarse-grained models, the solvent is typically taken into account either implicitly (using Langevin or Brownian dynamics) or on the mesoscopic level. These approaches are discussed next.

3.3. Langevin dynamics

If a spherical particle of mass m and radius a moves with velocity \mathbf{V} in a quiescent fluid of viscosity η , the collisions with the fluid give rise to two types of forces: a frictional

force $-\zeta\mathbf{V}$, where $\zeta = 6\pi\eta a$ is the friction coefficient, and a fluctuating stochastic force $\mathbf{F}_s(t)$ the magnitude of which is linked with ζ by a fluctuation–dissipation theorem

$$\langle \mathbf{F}_s(t)\mathbf{F}_s(t') \rangle = 2k_B T \zeta \delta(t - t') \mathbf{I}$$

where \mathbf{I} is the identity matrix and the term $\delta(t - t')$ reflects the fact that the random forces are uncorrelated on the scale of particle motion (however, see below). The dynamics of such a particle can then be described by the following Langevin equation:

$$m\ddot{\mathbf{R}} = -\zeta\dot{\mathbf{R}} + \mathbf{F}^e + \mathbf{F}_s \quad (1)$$

where \mathbf{R} is the position of the particle and \mathbf{F}^e is the net external force acting on it.

There is an important reservation, however. As already noted by Lorentz [59–61], the Langevin equation in the above form may only be used if there is a separation of time scales between the relaxation time of the particle (i.e. the bead) velocity $\tau_v = \frac{m}{\zeta} = \frac{2a^2\rho}{9\eta}$ and the viscous relaxation time of the solvent, $\tau_\eta = a^2 \frac{\rho_s}{\eta}$, where ρ is the density of the particle, and ρ_s the density of the solvent (see also the thorough discussion in the book by Mazo [60]). The ratio of these two time scales is proportional to ρ/ρ_s . Since the densities of proteins are only about 50% higher than those of the surrounding liquid [62], there is no clear separation of time scales between the relaxation of fluid variables and those of the bead, and on time scales $t \sim \tau_v \approx \tau_\eta$ instead of equation (1) one should use the generalized Langevin equation involving a memory kernel $\xi(t)$:

$$m\ddot{\mathbf{R}}(t) = - \int_0^t dt' \xi(t - t') \dot{\mathbf{r}}(t') + \mathbf{F}^e(t) + \mathbf{F}_s(t). \quad (2)$$

Here the noise is again Gaussian and related to the dissipative term through the generalized fluctuation–dissipation relation

$$\langle \mathbf{F}_s(t)\mathbf{F}_s(t') \rangle = k_B T \xi(t - t') \mathbf{I}.$$

Importantly, even though the results of the instantaneous Langevin equation (1) are not physical at time scales $t \sim \tau_\eta$, it may still be used to describe processes on time scales $t \gg \tau_\eta$. As shown in [51], on these time scales the Langevin approach (in the overdamped limit) gives results consistent with those of Brownian dynamics, which itself is not affected by solvent inertia effects [61].

3.4. Overdamped limit and Brownian dynamics

The magnitude of the inertial term in the Langevin equation (1) is given by mV/τ , where V is a characteristic velocity and τ a characteristic time scale of the dynamics. On the other hand, the magnitude of the friction term is given by ζV . The ratio of these two terms is simply τ_v/τ ; thus on the time scales $\tau \gg \tau_v$ the inertial term in (1) can be neglected.

The next observation is that in most of the soft matter systems the configurational evolution takes place on the time scales τ much longer than τ_v , hence the inertial effects are not important there and it is appropriate to describe the dynamics in terms of equilibration of the particle configurations only.

The exact definition of τ is problem-dependent: on the single-monomer level it is the time needed by a monomer to diffuse over its own size, $\tau_0 = a^2/D$ (where D is the diffusion constant and a the monomer radius). At the level of the chain as a whole, the respective time scales are even longer, with the Rouse relaxation time $\tau_R \sim \tau_0 N^2$ or the Zimm time $\tau_Z \sim \tau_0 N^{3/2}$ [63]. The configurational evolution of particles observed with a time resolution $\tau \gg \tau_v$ is usually referred to as Brownian dynamics and is described by the overdamped version of (1)

$$\dot{\mathbf{R}} = \frac{1}{\zeta} (\mathbf{F}^e + \mathbf{F}_s) = \frac{1}{\zeta} \mathbf{F}^e + \mathbf{B} \quad (3)$$

where the stochastic velocity component, \mathbf{B} , is a Gaussian random variable with zero mean and the covariance

$$\langle \mathbf{B}(t)\mathbf{B}(t') \rangle = \frac{2k_B T}{\zeta} \delta(t - t') \mathbf{I}. \quad (4)$$

As mentioned above, the Brownian dynamics describes configurational evolution of the beads on time scales in which the inertial effects of the beads and solvent molecules are negligible [61], and therefore time scale separation issues discussed in the previous section are not pertinent here.

3.5. Inclusion of flow and hydrodynamic interactions

It is relatively straightforward to generalize (3) to the case when the particle is immersed in a linear flow field

$$\mathbf{u}(\mathbf{r}) = \mathbf{u}_0 + \mathbf{K} \cdot \mathbf{r}. \quad (5)$$

where \mathbf{K} is the velocity gradient matrix [64].

Namely, one uses Faxen's theorem [64, 65] for a spherical particle

$$\mathbf{V} = \frac{1}{\zeta} \mathbf{F} + \mathbf{u}(\mathbf{R}) + \frac{1}{6} a^2 \nabla_{\mathbf{R}}^2 \mathbf{u}(\mathbf{R}), \quad (6)$$

where \mathbf{V} is the velocity of the particle, \mathbf{F} is a net force acting on it, \mathbf{R} is the position of its center and $\nabla_{\mathbf{R}}^2$ is a Laplace operator with respect to \mathbf{R} . For a linear field (5) the above leads to a simple conclusion that

$$\mathbf{V} = \mathbf{u}(\mathbf{R}) + \frac{1}{\zeta} \mathbf{F} \quad (7)$$

and the (single-particle) Brownian dynamics equation (3) is then generalized to the form

$$\dot{\mathbf{R}} = \mathbf{u}(\mathbf{R}) + \frac{1}{\zeta} (\mathbf{F}^e + \mathbf{F}_s) = \mathbf{u}(\mathbf{R}) + \frac{1}{\zeta} \mathbf{F}^e + \mathbf{B}. \quad (8)$$

If there are many particles in the system, the situation gets considerably more complicated, since the motion of one particle induces a flow which acts on all the other particles. The hydrodynamic interactions are truly complex: they are long ranged, nonlinear in nature, and cannot be expressed as a sum of two-body terms. With the inclusion of hydrodynamic interactions, the Brownian dynamics scheme takes the following form [66–69, 64]

$$\begin{aligned} \mathbf{R}_i(t + \Delta t) &= \mathbf{R}_i(t) + \mathbf{u}_0 \Delta t + \mathbf{K} \cdot \mathbf{R}_i(t) \Delta t \\ &+ \sum_j (\nabla_j \cdot \mathbf{D}_{ij}) \Delta t + \frac{1}{k_B T} \sum_j \mathbf{D}_{ij} \cdot \mathbf{F}_j^e \Delta t \\ &+ \mathbf{C}_i : \mathbf{K} \Delta t + \mathbf{F}_i. \end{aligned} \quad (9)$$

Here \mathbf{R}_i is the position of the i th particle, \mathbf{F}_i^c is the total external force acting on it and \mathbf{D} is the diffusion tensor. Both \mathbf{F} and \mathbf{D} are configuration-dependent and are evaluated at the beginning of the timestep. Next, $\mathbf{\Gamma}$ is a random displacement given by a Gaussian distribution with an average value of zero and covariance obeying

$$\langle \mathbf{\Gamma}_i \mathbf{\Gamma}_j \rangle = 2\mathbf{D}_{ij} \Delta t. \quad (10)$$

Finally, \mathbf{C} is the third rank shear disturbance tensor [64] representing the effect of interparticle hydrodynamic forces on the shear-induced particle motion [67, 69], also evaluated at the beginning of the timestep.

In general, the diffusion tensor \mathbf{D} depends in a complicated nonlinear way on the instantaneous positions of all particles in the system. For a system of spheres, exact explicit expressions for the diffusion tensor \mathbf{D}_{ij} exist in the form of the power series in interparticle distances, which may be incorporated into the simulation scheme [65, 67, 70–74]. In polymer modeling, for numerical tractability, the diffusion matrix is often approximated by its far-field asymptotes. The lowest order of approximation (first order in a/R_{ij}) corresponds to the Oseen tensor

$$\frac{1}{k_B T} \mathbf{D}_{ij} = \frac{1}{\zeta} \left(\mathbf{I} \delta_{ij} + \frac{3}{4} \frac{a}{R_{ij}} (\mathbf{I} + \hat{\mathbf{R}}_{ij} \hat{\mathbf{R}}_{ij}) (1 - \delta_{ij}) \right) \quad (11)$$

and is equivalent to treating the particles as point forces (Stokeslets) in the viscous fluid. The off-diagonal components of this tensor, \mathbf{D}_{ij} with $i \neq j$, describe the contribution of the force acting on particle j to the velocity of particle i .

The next level of approximation (retaining the terms up to $(a/R_{ij})^3$) corresponds to the Rotne–Prager tensor [75]. It is usually supplemented with a regularization for $R_{ij} < 2a$ proposed by Yamakawa [75, 76]. Together, this constitutes the so-called Rotne–Prager–Yamakawa tensor with the off-diagonal elements of \mathbf{D}_{ij} given by

$$\frac{1}{k_B T} \mathbf{D}_{ij} = \frac{1}{8\pi\eta R_{ij}} \begin{cases} \left[\left(1 + \frac{2a^2}{3R_{ij}^2} \right) \mathbf{I} + \left(1 - \frac{2a^2}{R_{ij}^2} \right) \right. \\ \left. \times \hat{\mathbf{R}}_{ij} \hat{\mathbf{R}}_{ij} \right], & R_{ij} \geq 2a \\ \frac{R_{ij}}{2a} \left[\left(\frac{8}{3} - \frac{3R_{ij}}{4a} \right) \mathbf{I} \right. \\ \left. + \frac{R_{ij}}{4a} \hat{\mathbf{R}}_{ij} \hat{\mathbf{R}}_{ij} \right], & R_{ij} < 2a. \end{cases} \quad (12)$$

In both the Oseen and Rotne–Prager–Yamakawa approximations, the divergence of the diffusion matrix vanishes ($\sum_j \nabla_j \cdot \mathbf{D}_{ij} \equiv 0$), which further simplifies the numerical scheme. However, if the full hydrodynamic interactions are included, the divergence term should be taken into account [77].

Finally, at this level of approximation (up to $(a/R_{ij})^3$), the shear disturbance tensor is given by [64]

$$\mathbf{C} = -\frac{5}{2} \sum_{j \neq i} (a/R_{ij})^3 \hat{\mathbf{R}}_{ij} \hat{\mathbf{R}}_{ij} \mathbf{R}_{ij}. \quad (13)$$

Note that at the level of Oseen hydrodynamics, the shear disturbance tensor is zero and the only effect of the shear field on the system is through the velocity field $\mathbf{u}(\mathbf{r})$ itself.

Finally, the above considerations are based on the assumption that the fluid is of an infinite extent. When studying fluids in confined spaces, or in the presence of surfaces, the diffusion tensor has to account for the stick boundary conditions at the walls, which makes the derivation considerably harder [78]. Some of the geometries are well studied, with the expressions for the full diffusion tensor derived. The examples include soft matter systems near a single wall [79] and between two walls [80]. This formalism can then be applied to study problems like binding of blood-borne cells to the vessel walls [81], interaction of cytochrome c molecules with a negatively charged lipid bilayer [82] or cargo-transport of kinesin-like processive motors [83]. In other geometries only the lowest order, Stokeslet solution are known, e.g. in cylindrical [84] or spherical [85] geometry. The latter was used to analyze effects of hydrodynamic interactions on protein folding in confined and crowded spaces [86].

When taking the hydrodynamic interactions into account, the choice of a hydrodynamic radius, a , is a crucial element in the model. One of the ways of tuning this parameter is to compare the translational diffusion coefficient, D , of a protein in a numerical model to the one measured in experiments. In [52] we have compared the experimental data on the diffusion coefficient of ubiquitin [87] with the numerically obtained D for various hydrodynamic radii and found agreement for $a \approx 4.1$ Å. This value agrees with earlier estimates by de la Torre and Antosiewicz [88–92]. On the other hand Frembgen-Kesner and Elcock use $a = 5.3$ Å in their studies of protein folding with a Go-type model without side groups (and $a = 3.5$ Å for the model with side groups).

However, since the distance between the successive C^α atoms along the protein backbone is 3.8 Å, some of the beads representing amino acids overlap. This reflects the fact that: (1) the interior of the protein is densely packed, (2) the side chains of amino acids are usually longer than 3.8 Å, and (3) the protein is covered by a hydration layer of tightly bound water molecules. Although the Rotne–Prager–Yamakawa tensor is also positively defined for overlapping beads, its physical meaning for such configurations is problematic [91]. The overlapping bead models are successful in predicting the diffusion coefficients of the proteins [88, 89]; however, the question of whether they correctly reproduce the dynamic effects of hydrodynamic interactions during large-scale conformational motions in macromolecules is still open. Interestingly, in a different, non-hydrodynamic, context the overlapping bead models were shown to introduce an inherent tube-like anisotropy which is responsible for protein-like behavior in the chains of beads [93].

Finally, it is worth mentioning that implicit solvent, Brownian dynamics models give the unique opportunity to separate HI-associated effects in the dynamics from those of other factors. To this end, one performs the simulations twice—with and without HI included. In the second case, one uses simply a diagonal diffusion matrix

$$\frac{1}{k_B T} \mathbf{D}_{ij} = \frac{1}{\zeta} \mathbf{I} \delta_{ij}. \quad (14)$$

The differences between the two runs, if any, can then be unambiguously attributed to the effect of hydrodynamic interactions.

3.6. Mesoscopic solvent models

Another approach to modeling hydrodynamic effects in biopolymers is to use mesoscopic models for the solvent dynamics. The basic idea here is to track the solvent degrees of freedom through a simplified mesoscopic representation, with the local dynamics that satisfies the mass, momentum and energy conservation laws and recovers the solution of hydrodynamic equations in the large-scale limit. Several algorithms of that kind have been developed over the last 20 years, and the most widely used nowadays are:

- (i) The lattice-Boltzmann method, in which populations of particle densities move synchronously, according to discrete time steps, along the links of a regular lattice. When bouncing into each other, these densities are redistributed among the lattice directions in such a way that mass and momentum are conserved.
- (ii) Multi-particle collision dynamics (also called stochastic rotation dynamics), in which the fluid is modeled as a collection of particles whose positions and velocities are continuous variables. The system is coarse-grained into cells and the dynamics consists of two steps: free streaming, when the particles move ballistically and do not interact, and collisions which are modeled by a simultaneous stochastic rotation of the relative velocities of every particle in a each cell.

In order to simulate a soft matter system, the solvent model must then be coupled with the respective algorithms that models the dynamics of solute particles. A detailed discussion of these approaches is beyond the scope of this review, and the reader is referred to other articles, e.g. the recent reviews [94–96].

The main advantage of mesoscale methods is their spatial locality, which results in a $O(N)$ scaling of computational complexity with a number of particles, and the main disadvantage is an introduction of additional degrees of freedom and short time scales that need to be resolved [96]. Importantly, in these models hydrodynamic interactions between the particles arise intrinsically, due to the explicit coupling between the moving particle surfaces and the solvent. This, together with simplicity of implementation of complex boundary conditions, constitutes the reason why mesoscopic solvent algorithms are often used to analyze the hydrodynamic effects in complex confining geometries.

Mesosopic methods have been successfully applied to biopolymer dynamics problems (see e.g. [97–99]). In the context of protein dynamics, Kikuchi *et al* [48] and Ryder [49] have used stochastic rotation dynamics to analyze the influence of HI on protein folding.

3.7. Other computational approaches

Lemak *et al* in their studies of protein unfolding in uniform and elongational flows [55, 56] have used a ‘collision molecular-dynamics’ method [100], in which each amino acid collides with virtual solvent particles. Post-collision velocities are calculated by solving the collision problem, in which the velocity of a virtual solvent particle is drawn randomly from the Maxwellian distribution centered around the hydrodynamic velocity of a solvent at a given point. A main deficiency of that method is that ignores the correlations between solute–solvent collisions at different spatial points, thus hydrodynamic interaction effects are not taken into account here.

4. Numerical studies of flow-induced conformational changes in proteins

Despite a growing number of experimental investigations, computational studies on proteins in hydrodynamic flows are still rather scarce. The first two papers on the subject, by Lemak *et al* appeared in 2003 [55, 56] and were devoted to the analysis of forced unfolding of α -helix bundles and β -sheet barrels in uniform and elongational flows. The 3D elongational flow considered there is the flow pattern corresponding to a strong stretching in the one spatial direction and contraction in the remaining two:

$$\begin{aligned} u_x &= \dot{\gamma}(x - x_0), & u_y &= -\frac{1}{2}\dot{\gamma}(y - y_0), \\ u_z &= -\frac{1}{2}\dot{\gamma}(z - z_0), \end{aligned} \quad (15)$$

where (x_0, y_0, z_0) corresponds to a location of the stagnation point for the flow. In [55, 56] the authors observed a number of metastable, intermediate structures in uniform flow unfolding but no intermediates in the case of elongational flow. Subsequent studies by the authors of the present survey [50] have confirmed these findings. They have also provided a detailed comparison between unfolding by the flow and that by a mechanical force. It turns out that unfolding in a flow shows a larger number of intermediates than AFM force-clamp unfolding. If the flow rate is sufficiently low, the protein may remain trapped in one of these states for the duration of the simulation. Additionally, one observes different unfolding pathways and different sets of intermediate states depending on which terminus in the protein is tethered. Also, the flow magnitude needed for the full unwinding of a protein chain is attachment-dependent. This observation can be explained by noting that the tension along the tethered protein chain in the flow is highly non-uniform: it increases starting from the free end towards the tethered end (cf section 5). Thus, in flow-induced unfolding, the bonds in the vicinity of the tethered terminus are broken first, which is in contrast to AFM-mediated unfolding when it is the weakest link which will snap first. Hence, by changing the attachment points of the protein in the flow one can probe different patches of its energetic landscape. These features offer potentially wider diagnostic tools to investigate structure of proteins than experiments based on AFM.

In the case of homopolymers, the interplay of an increasing tension along the tethered chain in the flow

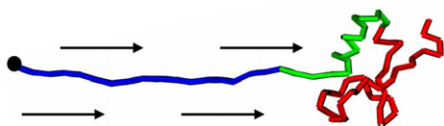


Figure 1. Example conformation of a tethered ubiquitin in a uniform flow.

and thermal fluctuations leads to a characteristic ‘trumpet-like’ shape of a polymer in the flow [101, 102]. Closer analysis [103] leads to the conclusion that there are in fact several conformational regimes, depending on the magnitude of the flow field. At low flows, the chain can be modeled as a weakly distorted coil while at higher velocities a trumpet-like shape is attained, with the chain becoming more unwound towards the tethered end. With a further increase in the flow the fraction of the polymer near a fixed end becomes completely stretched and forms a ‘stem’, ending in a fluctuating coil, the ‘flower’. In the case of protein in the flow, this simple picture is complicated by the presence of cross-linking contacts between amino acids. In that case, instead of a smooth, trumpet-like profile of the coiled part, the part of protein near the free terminus attains a specific, energetically favorable, metastable conformation, as illustrated in figure 1.

Szymczak and Cieplak [52] have also analyzed the process of protein unfolding by shear flow. As already mentioned, shear flow is particularly attractive for experimentalists, and indeed most experiments on flow-induced effects on proteins were carried out with that type of a flow. As already noted by Lumley [104] and de Gennes [105], a notable feature of shear flow is that it is a combination of elongational and rotational components of equal magnitude. In such a marginal case the polymer chain does not attain a stable stretched configuration. Instead, it undergoes a tumbling motion, a series of subsequent stretching and coiling events with frequent

changes in the orientation of the chain with respect to the shear axis [106–109]. While the elongational component of the flow is stretching the molecule, its rotational component aligns it along the shear axis, leading to the collapse of the chain due to the decreased hydrodynamic drag. An important role in this dynamics is played by Brownian fluctuations, which cause the chain segments to cross the streamlines into the regions of higher or lower flow which results in further stretching or collapse of the chain, respectively. In particular, the fluctuations may tip the polymer in such a way that its two ends lie in the regions of opposite flow direction, which results in a tumbling event, in which one polymer end moves over the other.

A similar tumbling dynamics of protein molecules was observed in the simulations reported in [52] (cf figure 2). However, the presence of a complex network of bonds between amino acids in a protein results in a number of important differences between the homopolymer and protein unfolding in hydrodynamic flows. In particular, the extension of the protein in a uniform flow is not a continuous function of the flow rate. Instead, as the flow velocity is increased, the protein undergoes a number of rapid transitions to successive, metastable states, an example of which is shown in figure 1. Each of these transitions is accompanied by the breaking of a particular group of bonds and unzipping of subsequent structures from the bulk of the protein. In contrast to uniform flow, in a shear flow these states are never long-lived, even a small thermal fluctuation may move the protein to a region of lower flow and the chain collapses.

Another interesting feature of a protein’s dynamics in a shear flow is its relatively complex spectrum of an orientation angle (defined as an angle between the end-to-end direction of the protein and the direction of the flow). Namely, two peaks can be identified in the spectrum, corresponding to two characteristic tumbling frequencies [52]. The higher frequency is the one associated with the rotational component of the shear

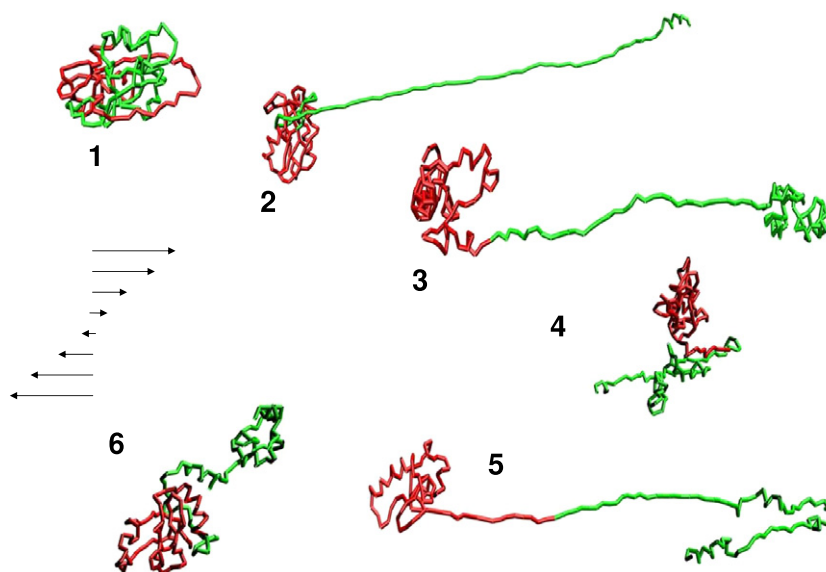


Figure 2. Example of a tumbling cycle of a protein in a shear flow: integrin at $Wi = 3200$. For tracing purposes, the two halves of the chain are marked in different colors/shades of grey.

flow, $f_1 = \frac{\dot{\gamma}}{4\pi}$ (a sphere immersed in the shear field rotates with the frequency f_1 [64]). On the other hand, the lower frequency, f_2 , corresponds to the stretching–collapse cycle and scales sublinearly ($f_2 \sim \dot{\gamma}^{2/3}$) with the shear rate, similar to what was reported in DNA experiments [109]. As noted by Kobayashi and Yamamoto [110], the coexistence of these two frequencies is a unique property of proteins due to the presence of cross-linking contacts between the amino acids, which gives the protein the ability to fold into a compact shape. For a homopolymer chain in a steady shear flow both frequencies are also observed, but in different shear regimes, and they never coexist [110].

Finally, we come back to the problem of ambiguous experimental results on the shear flow unfolding of proteins. The Brownian dynamics results reported in [52] show that the minimal shear rate needed to initiate the stretching–collapse cycle corresponds to the Weissenberg number of about $5 \times 10^2 - 2 \times 10^3$, which agrees with the theoretical estimate of Jaspé and Hagen [3]. However, even at larger shear rates, the protein never unfolds completely, but rather constantly undergoes collapse–stretch cycles, which may partially explain seemingly contradictory experimental data on shear-induced unfolding.

Other important theoretical studies on shear-induced conformational changes in proteins are those of Schneider *et al* [15] and Alexander-Katz *et al* [14, 111], which accompanied their experimental work on the unfolding of vWf globules [15]. As already mentioned, the main interest here was the quaternary structural changes. In fact, in the numerical model adopted in [15, 111] successive vWf protein domains in the multi-unit chain were approximated by single beads, so that the tertiary structure was not resolved. Nevertheless, a number of important insights into the physics of shear-induced unfolding were provided by the analysis. Most importantly, they identified a new mechanism for the shear-induced instability of collapsed globules in the shear flow associated with the presence of thermally excited polymeric protrusions on the interface between a collapsed polymer phase and a viscous solvent. This has allowed them to estimate the critical shear rate needed for the initiation of coil–stretch cycles. An analogous approach was then applied to the case of elongational flow [112] and the corresponding threshold fold rate needed to stretch the molecule was estimated. Although these results are not directly applicable to the case of unfolding of single protein tertiary structure, due to the presence of a highly ordered network of cross-linked bonds in the latter, one can expect that the protrusion-associated instability may also play an important role here (cf the discussion in the appendix).

Finally, let us briefly discuss two pioneering studies of protein unfolding in uniform flow performed at atomic resolution, already mentioned in section 3.1. First, Chen *et al* [21, 22] have revealed that flow induces a transition from an unstructured loop to a β -hairpin in the 16-residue β -switch region of platelet glycoprotein Ib. It is an important result, since this region is involved in contact between glycoprotein Ib and vWf. Hence the reported flow-induced conformational changes might provide a regulatory mechanism for platelet adhesion to vWf.

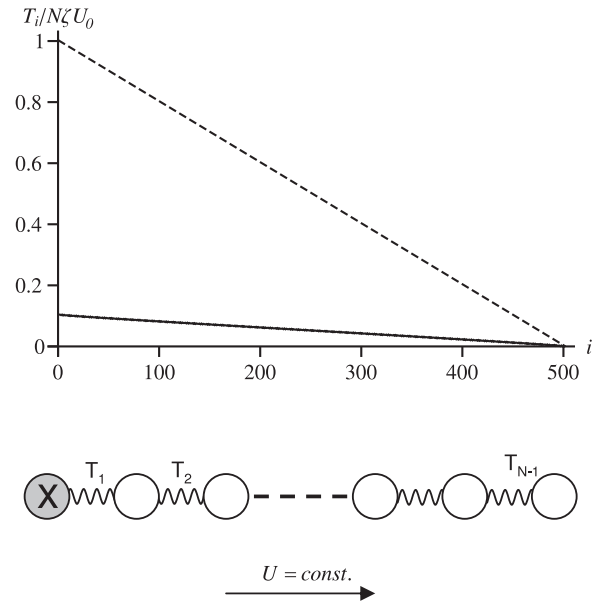


Figure 3. The distribution of tension along the chain in a uniform flow with (solid) and without (dashed) hydrodynamic interactions. The first bead (marked in gray) is tethered. The total number of beads in the chain is $N = 500$ and $l/a = 2$.

Next, Wang and Sandberg [41] have analyzed ubiquitin unfolding in a uniform flow and compared the results to those of coarse-grained models with an implicit solvent [50]. Due to the atomistic resolution, they were able to resolve very short time scales in protein dynamics, on which the effects of both protein and solvent inertia become important. However, due to very high flow rates used in that study to unfold the protein (180 m s^{-1}), it is not entirely obvious whether these effects can indeed be observed in a real experimental situation. On the other hand, for the smaller speeds simulated in [41] (0.18 m s^{-1}) the authors found no unfolding, which is was presumably due to too short a timespan covered by the simulation ($\sim 1 \text{ ns}$).

5. Flow-induced tension along the chain

As mentioned above, the main difference between protein unfolding by a mechanical force and that induced by flow is the fact that a flow generates a non-uniform tension along the molecule. Let us elucidate this point with a simple example. Specifically, we consider an extended chain comprising equally spaced beads connected with springs, aligned parallel to the flow direction (\mathbf{e}_x) as illustrated in figure 3. The first bead is tethered and the molecule as a whole does not move, i.e. $\dot{\mathbf{R}}_i = 0$, for $i = 1, \dots, N$. Moreover, since the successive beads are aligned along X we get $\hat{\mathbf{R}}_i \hat{\mathbf{R}}_j = \mathbf{e}_x \mathbf{e}_x$ and $\mathbf{F}_i = F_i \mathbf{e}_x$. The Oseen contribution to the particle velocity takes then the form

$$\left(\frac{1}{k_B T} \mathbf{D}_{ij} \mathbf{F}_j \right)_x = \frac{1}{\zeta} \left(\delta_{ij} + \frac{3}{2} \frac{a}{l|i-j|} (1 - \delta_{ij}) \right) F_j \quad (16)$$

where l is the distance between the successive beads. On using (9), the condition of vanishing velocity can then be

written as the following matrix equation:

$$\hat{A}\mathcal{F} = -\zeta\mathcal{U}_0 \quad (17)$$

where $\mathcal{F} = (F_1, \dots, F_N), \mathcal{U} = (U_0, \dots, U_0)$ and

$$\hat{A}_{ij} = \delta_{ij} + \frac{3}{2} \frac{a}{l|i-j|} (1 - \delta_{ij}), \quad (18)$$

where we neglected the divergence of the diffusion matrix, since the hydrodynamics is taken into account here at the Oseen level. However, the forces on the particles can be expressed in terms of the tensions of successive springs: $F_1 = T_1; F_2 = T_2 - T_1, \dots, F_N = -T_{N-1}$, or, in the matrix form

$$\mathcal{F} = \hat{B}\mathcal{T}, \quad (19)$$

where $\mathcal{T} = (T_1, \dots, T_{N-1})$ and

$$\hat{B} = \begin{bmatrix} 1 & & & \\ -1 & 1 & & \\ & & \dots & \\ & & & -1 \end{bmatrix}. \quad (20)$$

Finally,

$$\hat{A}\hat{B}\mathcal{T} = -\zeta\mathcal{U}_0 \quad (21)$$

which can then be solved to yield the tensions, T_i , in successive springs. Figure 3 presents the tension profiles for a $N = 500$ -bead chain both with and without hydrodynamic interactions. In the latter case, equation (21) can be solved analytically to yield a linear profile

$$T_i = (N - i)\zeta U_0, \quad i = 1, \dots, N - 1. \quad (22)$$

With HI included, the tension is much weaker, but the profile remains nearly linear. For long chains, the tension in the first spring is well approximated by $\zeta_r U_0$, where $\zeta_r = 2\pi l(N - 1)\eta / \ln[l(N - 1)/2a]$ is the friction coefficient of a rod of length $l(N - 1)$ and width $2a$ [113], thus in this case

$$T_i = (N - i)2\pi l\eta U_0 / \ln[l(N - 1)/2a], \quad i = 1, \dots, N - 1. \quad (23)$$

The same reasoning can be repeated for the case of elongational flow, $u_x = \dot{\gamma}x$, with the only difference being that the velocity vector \mathcal{U} is now given by

$$\mathcal{U}_i = \dot{\gamma}l(i - (N + 1)/2). \quad (24)$$

The respective tension profiles are shown in figure 4. Without HI, we get a parabolic profile of the form

$$T_i = \frac{1}{2}i(N - i)\zeta\dot{\gamma}l, \quad i = 1, \dots, N - 1. \quad (25)$$

Again, with HI included, the tension is much weaker, but the profile remains parabolic. Similar to the case of a uniform flow, for long chains the HI results can be approximated [114, 27] by the slender rod theory

$$T_i = \pi\eta l^2\dot{\gamma}i(N - i) / \ln[l(N - 1)/4a], \quad i = 1, \dots, N - 1. \quad (26)$$

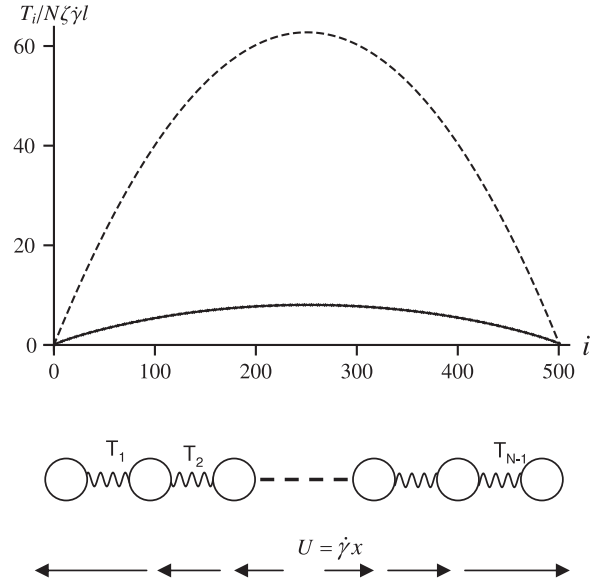


Figure 4. The distribution of tension along the chain in an elongational flow with (solid) and without (dashed) hydrodynamic interactions. The total number of beads in the chain is $N = 500$ and $l/a = 2$.

There are several points to be noted in this context:

- (i) Hydrodynamic interactions decrease the flow-induced tension along the chain considerably. However, as noted by de Gennes [115], in an elongated molecule, HI change only the absolute value of the tension not the form of the profile itself.
- (ii) The effect of elongational flow on long molecules is much stronger than that of uniform flow. In the former case, the highest tension scales as N^2 with the number of beads and in the latter as N .
- (iii) The estimates of the tension given above are obtained for the elongated, linear molecules. In the case of tightly packed, spherical shapes, the tension in the bonds between the beads becomes much weaker, since the drag is limited to the beads remaining on the surface; those inside the globule are almost entirely screened from the flow if HI are included in the description of the system (see also the discussion in section 6 and figure 6).
- (iv) Even though the shear flow has an elongational component, its impact on the molecules is usually much weaker than that of the pure elongational flow of equation (15); this is because of the presence of a rotational component in the shear flow. Rotation leads the molecule out of the region of the strongest elongation, and it contracts again. Thus the molecule is exposed to peak elongation intermittently during each tumbling cycle. On the other hand, stretching by a pure elongational flow (15) is usually a transient phenomenon: typically, the molecule is exposed to it as it passes constrictions in capillaries.

6. Effects of hydrodynamic interactions on protein unfolding

Hydrodynamic effects in protein dynamics are not necessarily due to any external flows acting on a biomolecule. Even in

the absence of external flow, different segments of a protein excite long-ranged flows as they move, which then influence all other segments. By generating the flow and reacting to it, the segments experience hydrodynamic interactions with each other and with the walls of the container. The presence of HI is known to affect the dynamic properties of soft matter. For instance, HI modify the values of diffusion coefficients in colloidal suspensions [64], affect the characteristics of the coil–stretch transition in polymers [116], play a key role in collective swimming at low Reynolds numbers [117], and control a concerted motion of microorganisms near the surface [118] or intricate periodic trajectories of sedimenting particles [119].

Much less is known about the role of HI in protein folding and unfolding processes. Dickinson [120] and Tanaka [121] speculated that HI might affect the kinetics of protein folding, but an actual numerical assessment of the role of HI has come with the paper by Baumketner and Hiwatari [58]. They have considered coarse-grained models and found that HI delay folding of a β -hairpin but do not affect folding of the α -helix. Kikuchi *et al* [48] has found that HI have a negligible effect on protein folding, whereas Ryder [49] reported a small, of the order of 10%, reduction in the folding time in simple models of several proteins, such as 2ci2. A stronger effect of HI on folding was observed by Cieplak and Niewieczerzal [54], who reported speed-up by about a factor of 1.3–2.3, depending on the particular protein. Similar speed-up has been reported by Frembgen-Kesner and Elcock [53], who analyzed the folding dynamics of 11 proteins and found that—depending on the protein model adopted—HI increase the folding rate by the average factor of 1.7 for the Go-type model without side groups and 3.07 for the model with side groups. Interestingly, they also reported an HI-associated decrease in folding rates of the individual secondary structures (α -helices and β -hairpins). They hypothesized that HI accelerate the formation of non-local interactions while at the same time decelerating the formation of local interactions.

The differences in results between the authors on HI effects in protein folding might be partially connected to the nature of the starting conformations (statistically independent swollen chain configurations were used as initial conformations in [48, 49], whereas extended, linear configurations were used in [54]), different folding criteria and differences in the coarse-grained protein model used. A significant role played by the ensemble of initial configurations was further confirmed in [86], where it was shown that the more tightly packed the set of initial protein conformations is, the smaller the differences between folding times with and without HI. This can be rationalized by noting that HI significantly speed up the initial, collapse phase of the folding process [54, 53], analogous to a similar phenomenon in homopolymers [48, 122, 123]. However, the subsequent establishment of contacts involves a stochastic search in the conformational space and is not affected by any hydrodynamic effects. For extended initial conformations, the collapse phase is longer and more pronounced than in the case of tighter conformations, hence the stronger effect of HI. Interestingly, the folding pathways do not seem to be affected by the

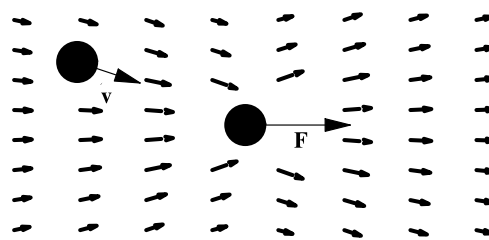


Figure 5. The dragging effect: the moving particle creates a flow pattern which affects other particles by pulling them in the direction of its motion (reprinted with permission from [51]. Copyright 2007 IOP Publishing.).

presence of hydrodynamic interactions [54], which also agrees with a similar observation for homopolymer collapse [123], where the collapse pathways from a good solvent state to a poor solvent state were found to be independent of hydrodynamic interactions, even though the collapse rates itself are significantly higher for the systems with HI.

In the case of mechanically induced unfolding, the impact of HI has been shown to depend on the way the protein is stretched. In a standard constant-velocity unfolding, usually carried out with use of an AFM, hydrodynamic effects were shown to play a minor role if the unfolding speeds are low enough [51]. However, for larger speeds (starting from about 0.5 \AA ns^{-1}) HI were shown to reduce the peak forces during stretching. Such speeds, although not relevant experimentally, are often used in numerical simulations, particularly in all-atom models.

For stretching at a constant force, the inclusion of HI changes the dynamics considerably [51]. The average unfolding times in the model with HI are much shorter than the results for the model without HI. Additionally, the unfolding pathways are different between the two models, particularly at higher forces. The fact that the HI facilitate protein unfolding was attributed to the so-called dragging effect: an amino acid pulled away from the bulk of a protein creates a flow which drags other residues with it (cf figure 5).

Finally, in flow-induced unfolding, either in a uniform [51] or in a shear flow [52], HI were shown to play a hindering role: unfolding of the system with HI requires a much larger flow speed than without. This can be understood qualitatively in terms of the so-called no-draining effect [124, 50]: the residues hidden inside the protein are shielded from the flow and thus only a small fraction of the residues experience the full drag force (see figure 6). In contrast, when no HI are present, this drag force is applied to all residues. In fact, an analogous shielding effect is the reason why values of the tension in the chains considered in figures 3 and 4 are much lower for the model with HI included than without.

7. Summary

In summary, we have briefly reviewed recent experimental and numerical studies on flow-induced effects in protein dynamics. Understanding the behavior of proteins in flows is crucial, not only for the development of new tools for

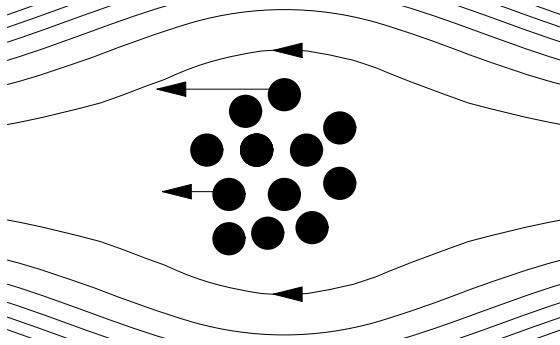


Figure 6. The shielding effect: the particles inside a cluster experience a smaller drag force than those on the surface (reprinted with permission from [51]. Copyright 2007 IOP Publishing.).

probing the conformational landscape of proteins, but also for understanding of many *in vivo* processes, such as hemostasis or ion channel activation. The presence of the solvent must also be taken into account to predict the time scales of conformational changes of protein structure correctly—in the case of both folding and unfolding of proteins.

Acknowledgments

This work has been supported by the grant N N202 0852 33 from the Ministry of Science and Higher Education in Poland, the EC FUNMOL project under FP7-NMP-2007-SMALL-1, and by the European Union within the European Regional Development Fund, through grant Innovative Economy (POIG.01.01.02-00-008/08).

Appendix. Estimate of the critical strain rate

Here we quote the estimate of the critical shear rate needed to denature a protein, as elaborated in [3]. In this approach, the unfolding protein in the elongational flow $v_x = \dot{\gamma}x$ is modeled by two roughly equal-sized coils of radius a separated by a straight linker of n amino acids oriented parallel to the x -axis, as illustrated in figure A.1. The tension along the chain due to the drag force experienced by each coil is then

$$T(n) = 3\pi\eta ad\dot{\gamma} \quad (\text{A.1})$$

where $d = 3.8 \text{ \AA}$ is the distance between consecutive amino acids along the chain. Since the proteins are tightly packed [125] the radius of each coil (a) is linked with the number of amino acids it comprises (m) by the relation $a^3 = mb^3$, where b is the average radius of an amino acid. The net work done by the fluid in completely separating the two clusters is then

$$W = 3\pi\eta d^2 \dot{\gamma} b \int_0^N n \left(\frac{N-n}{2} \right)^{1/3} dn = \frac{27}{28} 2^{-1/3} \pi \eta d^2 \dot{\gamma} b N^{7/3} \quad (\text{A.2})$$

where N is the total number of amino acids in the protein. Comparing W with the free energy of unfolding ($\Delta G \sim$

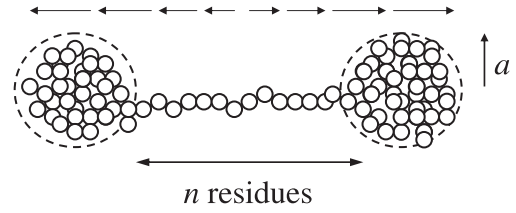


Figure A.1. A simple model of protein unfolding in elongational flow considered in [3].

40 kJ mol^{-1} for cytochrome *c*) one gets a shear rate of $\dot{\gamma} = 10^7 \text{ s}^{-1}$ as the threshold needed for protein denaturation by the flow. Next, the authors of [3] estimate the corresponding Weissenberg number by multiplying the above estimate of $\dot{\gamma}$ by the collapse time of the unfolded cytochrome *c* to the compact, molten globule state $\tau_c \sim 50 \mu\text{s}$. This gives $Wi \sim 10^3$ as the threshold Weissenberg number.

There are several simplifying assumptions in the above calculation, most important of which is the neglect of the rotational component of the shear flow, which rotates the elongated chain towards the direction of zero stretch rate thereby dramatically reducing the denaturing force of the flow. The above estimate (as remarked by the authors themselves) is thus more appropriate for a purely elongational flow, whereas the shear flow can unfold the protein only transiently, inducing stretching–collapse cycle as discussed in section 4.

Another issue concerns the initiation of the unfolding process in the above model. Namely, since the inside of the protein globule is shielded from the flow, it seems unlikely that the stretching will begin by breaking a group of bonds deep inside the protein structure which would then lead to the formation of two clusters as depicted in figure A.1. Rather, it is expected that the denaturation will be initiated at the protein surface, by a mechanism similar to that described by Katz *et al* [14] (cf section 4)—when a protrusion appears on the interface between a protein globule and a viscous solvent, the shear force may pull it further away from the surface and initiate protein unfolding. The results of simulations of the proteins in the shear flow reported in [52] further confirm this scenario. A small loop of the protein chain is usually pulled up first, most often involving the amino acids close to one of the termini. In many instances such a protrusion is quickly pulled back into the globule, but from time to time the whole loop with a terminus is pulled out (cf panel 2 in figure 2). Only then, after the rotation of the chain, might the terminal part be folded back which leads to a characteristic two-cluster shape, as seen in the third panel of figure 2.

References

- [1] Gregory R B 1995 *Protein–Solvent Interactions* (New York: Dekker)
- [2] Pal S K, Peon J and Zewail A H 2002 Biological water at the protein surface: dynamical solvation probed directly with femtosecond resolution *Proc. Natl Acad. Sci. USA* **99** 1763–8
- [3] Jaspe J and Hagen S J 2006 Do protein molecules unfold in a simple shear flow? *Biophys. J.* **91** 3415–24

- [4] Ashton L, Dusting J, Imomoh E, Balabani S and Blanch E 2009 Shear-induced unfolding of lysozyme monitored *in situ* *Biophys. J.* **96** 4231–6
- [5] Charm S E and Wong B L 1970 Enzyme inactivation with shearing *Biotechnol. Bioeng.* **12** 1103–9
- [6] Charm S E and Wong B L 1970 Shear degradation of fibrinogen in the circulation *Science* **170** 466–8
- [7] Thomas C R, Nienow A W and Dunhill P 1979 Action of shear on enzymes: studies with alcohol dehydrogenase *Biotechnol. Bioeng.* **21** 2263–78
- [8] Thomas C R and Dunhill P 1979 Action on shear on enzymes—studies with catalase and urase *Biotechnol. Bioeng.* **21** 2279–302
- [9] Maa Y-F and Hsu C C 1996 Effect of high shear on proteins *Biotechnol. Bioeng.* **51** 458–65
- [10] Maa Y-F and Hsu C C 1997 Protein denaturation by combined effect of shear and air–liquid interface *Biotechnol. Bioeng.* **54** 503–12
- [11] Edwards P J B, Kakubayashi M, Dykstra R, Pascals S M and Williams M A K 2010 Rheo-NMR studies of an enzymatic reaction: evidence of a shear-stable macromolecular system *Biophys. J.* **98** 1986–94
- [12] Bagci Z, Jernigan R L and Bahar I 1998 Biochemistry and genetics of von Willebrand factor *Annu. Rev. Biochem.* **67** 395–424
- [13] Siedlecki C A, Lestini B J, Kottke-Marchant K K, Eppel S J, Wilson D L and Marchant R E 1996 Shear-dependent changes in the three-dimensional structure of human von Willebrand factor *Blood* **88** 2939–50
- [14] Alexander-Katz A, Schneider M F, Schneider S W, Wixforth A and Netz R R 2006 Shear-flow-induced unfolding of polymeric globules *Phys. Rev. Lett.* **97** 138101
- [15] Schneider S W, Nuschele S, Wixforth A, Gorzelanny C, Alexander-Katz A, Netz R R and Schneider M F 2007 Shear-induced unfolding triggers adhesion of von Willebrand factor fibers *Proc. Natl Acad. Sci. USA* **104** 7899–903
- [16] Singh I, Themistou E, Porcar L and Neelamegham S 2009 Fluid shear induces conformation change in human blood protein von Willebrand factor in solution *Biophys. J.* **96** 2313–20
- [17] Choi H, Aboulfatova K, Pownall H J, Cook R and Dong J F 2007 Shear-induced disulfide bond formation regulates adhesion activity of von Willebrand factor *J. Biol. Chem.* **282** 35604
- [18] Goto S, Salomon D R, Ikeda Y and Ruggeri Z M 1995 Characterization of the unique mechanism mediating the shear-dependent binding of soluble von Willebrand factor to platelets *J. Biol. Chem.* **270** 23352
- [19] Arya M, Anvari B, Romo G M, Cruz M A, Dong J F, McIntire L V, Moake J L and Lopez J A 2002 Ultralarge multimers of von Willebrand factor form spontaneous high-strength bonds with the platelet glycoprotein Ib–IX complex: studies using optical tweezers *Blood* **99** 3971
- [20] Auton M, Cruz M A and Moake J 2007 Conformational stability and domain unfolding of the von Willebrand factor A domains *J. Mol. Biol.* **366** 986–1000
- [21] Lou J and Zhu C 2008 Flow induces loop-to- β -hairpin transition on the β -switch of platelet glycoprotein Ib α *Proc. Natl Acad. Sci. USA* **105** 13847–52
- [22] Chen Z, Lou J, Zhu C and Schulten K 2008 Flow-induced structural transition in the beta-switch region of glycoprotein Ib *Biophys. J.* **95** 1303–13
- [23] Kroll M H, Hellums J D, McIntire L V, Schafer A I and Moake J L 1996 Platelets and shear stress *Blood* **88** 1525–41
- [24] Colman R W, Hirsh J L, Marder J V, Clowes A W and George J N (ed) 2001 *Hemostasis and Thrombosis. Basic Principles and Clinical Practice* (Philadelphia, PA: Lippincott Williams & Wilkins)
- [25] Dong J-F, Moake J L, Nolasco L, Bernardo A, Arceneaux W, Shrimpton C N, Schade A J, McIntire L V, Fujikawa K and Lo A 2002 ADAMTS-13 rapidly cleaves newly secreted ultralarge von Willebrand factor multimers on the endothelial surface under flowing conditions *Blood* **100** 4033–9
- [26] Tsai H-M 2004 Molecular mechanisms in thrombotic thrombocytopenic purpura *Semin. Thromb. Hemost.* **30** 549–57
- [27] Zhang X, Halvorsen K, Zhang C-Z, Wong W P and Springer T 2009 Mechanoenzymatic cleavage of the ultralarge vascular protein von Willebrand factor *Science* **324** 1330–4
- [28] Sing C E and Alexander-Katz A 2010 Elongational flow induces the unfolding of von Willebrand factor at physiological flow rates *Biophys. J.* **98** L35–7
- [29] Hill E K, Krebs B, Goodall D G, Howlett G J and Dunstan D E 2006 Shear flow induces amyloid fibril formation *Biomacromolecules* **7** 10–3
- [30] Castelletto V and Hamley I W 2007 β -lactoglobulin fibers under capillary flow *Biomacromolecules* **8** 77–83
- [31] Bhak G, Lee J-H, Hahn J-S and Paik S R 2009 Granular assembly of α -synuclein leading to the accelerated amyloid fibril formation with shear stress *PLoS ONE* **4** e4177
- [32] Dunstan D E, Hamilton-Brown P, Asimakis P, Ducker W and Bertolini J 2009 Shear flow promotes amyloid-fibrilization *Protein Eng. Des. Sel.* **22** 741–6
- [33] Lokszejn A and Dzwolak W 2010 Vortex-induced formation of insulin amyloid superstructures probed by time-lapse atomic force microscopy and circular dichroism spectroscopy *J. Mol. Biol.* **395** 643–55
- [34] Lee J S, Um E, Park J-K and Park C B 2008 Microfluidic self-assembly of insulin monomers into amyloid fibrils on a solid surface *Langmuir* **24** 7068–71
- [35] Van Der Veen M E, Van Iersel D G, Van Der Goot A J and Boom R M 2004 Shear-induced inactivation of α -amylase in a plain shear field *Biotechnol. Prog.* **20** 1140–5
- [36] Olesen S P, Clapham D E and Davies P F 1988 Haemodynamic shear stress activates a K^+ current in vascular endothelial cells *Nature* **331** 168–70
- [37] Satlin L M, Sheng S, Woda C B and Kleyman T R 2001 Epithelial Na^+ channels are regulated by flow *Am. J. Physiol. Renal. Physiol.* **280** F1010–8
- [38] Carattino S, Sheng M D and Kleyman T R 2004 Epithelial Na^+ channels are activated by laminar shear stress *J. Biol. Chem.* **279** 4120–6
- [39] Althaus M, Bogdan R, Clauss W G and Fronius M 2007 Mechano-sensitivity of epithelial sodium channels (ENaCs): laminar shear stress increases ion channel open probability *FASEB J.* **21** 2389–99
- [40] Fronius W G and Clauss M 2008 Mechano-sensitivity of ENaC: may the (shear) force be with you *Pflügers Arch.* **455** 775–85
- [41] Wang G M and Sandberg W C 2010 Complete all-atom hydrodynamics of protein unfolding in uniform flow *Nanotechnology* **21** 235101
- [42] Veitshans T, Klimov D and Thirumalai D 1997 Protein folding kinetics: time scales, pathways and energy landscapes in terms of sequence-dependent properties *Folding Des.* **2** 1–22
- [43] Tozzini V 2005 Coarse-grained models for proteins *Curr. Opin. Struct. Biol.* **15** 144–50
- [44] Clementi C 2008 Coarse-grained models of protein folding: toy models or predictive tools? *Curr. Opin. Struct. Biol.* **18** 10–5

- [45] Hills R D Jr and Brooks C L III 2009 Insights from coarse-grained Go models for protein folding and dynamics *Int. J. Mol. Sci.* **10** 889–905
- [46] West D K, Brockwell D J, Olmsted P D, Radford S E and Paci E 2006 Mechanical resistance of proteins explained using simple molecular models *Biophys. J.* **90** 287–97
- [47] Sikora M, Sułkowska J I and Cieplak M 2009 Mechanical strength of 17 134 model proteins and cysteine slipknots *PLoS Comput. Biol.* **5** e1000547
- [48] Kikuchi N, Ryder J F, Pooley C M and Yeomans J M 2005 Kinetics of the polymer collapse transition: the role of hydrodynamics *Phys. Rev. E* **71** 1–8
- [49] Ryder J F 2005 Mesoscopic simulations of complex fluids *PhD Thesis* University of Oxford
- [50] Szymczak P and Cieplak M 2006 Stretching of proteins in a uniform flow *J. Chem. Phys.* **125** 164903
- [51] Szymczak P and Cieplak M 2007 Influence of hydrodynamic interactions on mechanical unfolding of proteins *J. Phys.: Condens. Matter* **19** 258224
- [52] Szymczak P and Cieplak M 2007 Proteins in a shear flow *J. Chem. Phys.* **127** 155106
- [53] Frembgen-Kesner T and Elcock A H 2009 Striking effects of hydrodynamic interactions on the simulated diffusion and folding of proteins *J. Chem. Theory Comput.* **5** 242–56
- [54] Cieplak M and Niewieczerzal S 2009 Hydrodynamic interactions in protein folding *J. Chem. Phys.* **130** 124906
- [55] Lemak A S, Lepock J R and Chen J Z Y 2003 Molecular dynamics simulations of a protein model in uniform and elongational flows *Proteins: Struct. Funct. Genet.* **51** 224–35
- [56] Lemak A S, Lepock J R and Chen J Z Y 2003 Unfolding proteins in an external field: can we always observe the intermediate states? *Phys. Rev. E* **67** 031910
- [57] Honeycutt J D and Thirumalai D 1992 The nature of folded states of globular proteins *Biopolymers* **32** 695–709
- [58] Baumketner A and Hiwatari Y 2002 Influence of hydrodynamic interaction on kinetics and thermodynamics of minimal protein models *J. Phys. Soc. Japan* **71** 3069
- [59] Lorentz H A 1927 *Lectures on Theoretical Physics* (London: Macmillan)
- [60] Mazo R M 2002 *Brownian Motion. Fluctuations, Dynamics, and Applications* (Oxford: Oxford Science)
- [61] Nägele G 2006 Brownian dynamics simulations *Computational Condensed Matter Physics*, vol B4:1, ed S Blügel, G Gompper, E Koch, H Müller-Krumbhaar, R Spatschek and R G Winkler (Jülich: Forschungszentrum)
- [62] Tsai J, Taylor R, Chotchia C and Gerstein M 1999 The packing density in proteins: standard radii and volumes *J. Mol. Biol.* **290** 253
- [63] Doi M and Edwards S F 1986 *The Theory of Polymer Dynamics* (Oxford: Oxford University Press)
- [64] Dhont J K G 1996 *An Introduction to Dynamics of Colloids* (Amsterdam: Elsevier)
- [65] Kim J H, Shi W-X and Larson R G 2007 Methods of stretching DNA molecules using flow fields *Langmuir* **23** 755–64
- [66] Ermak D L and McCammon J A 1978 Brownian dynamics with hydrodynamic interactions *J. Chem. Phys.* **69** 1352–60
- [67] Mazur P and van Saarloos W 1982 Many-sphere hydrodynamic interactions and mobilities in a suspension *Physica A* **115** 21–57
- [68] Ansell G C, Dickinson E and Ludvigsen M 1985 Brownian dynamics of colloidal-aggregate rotation and dissociation in shear flow *J. Chem. Soc. Faraday Trans.* **81** 1269
- [69] Bujan-Nunez M C and Dickinson E 1994 Brownian dynamics simulation of a multi-subunit deformable particle in simple shear flow *J. Chem. Soc. Faraday Trans.* **90** 2737–42
- [70] Durlofsky L, Brady J and Bossis G 1987 Dynamic simulation of hydrodynamically interacting particles *J. Fluid Mech.* **180** 21–49
- [71] Felderhof B U 1988 Many-body hydrodynamic interactions in suspensions *Physica A* **151** 1–16
- [72] Ladd A J C 1988 Hydrodynamic interactions in a suspension of spherical particles *J. Chem. Phys.* **88** 5051
- [73] Cichocki B, Felderhof B U, Hinsen K, Wajnryb E and Blawdziewicz J 1994 Friction and mobility of many spheres in Stokes flow *J. Chem. Phys.* **100** 3780–90
- [74] Phung T N, Brady J F and Bossis G 2006 Stokesian dynamics simulation of Brownian suspensions *J. Fluid Mech.* **313** 181–207
- [75] Rotne J and Prager S 1969 Variational treatment of hydrodynamic interaction in polymers *J. Chem. Phys.* **50** 4831
- [76] Yamakawa H 1970 Transport properties of polymer chains in dilute solution: hydrodynamic interaction *J. Chem. Phys.* **53** 436–43
- [77] Wajnryb E, Szymczak P and Cichocki B 2004 Brownian dynamics: divergence of mobility tensor *Physica A* **335** 339–58
- [78] Lee J 2004 Numerical simulation of complex fluids in confined geometries *PhD Thesis* University of Florida
- [79] Cichocki B and Jones R B 1998 Image representation of a spherical particle near a hard wall *Physica A* **258** 273–302
- [80] Bhattacharya S, Blawdziewicz J and Wajnryb E 2006 Hydrodynamic interactions of spherical particles in Poiseuille flow between two parallel walls *Phys. Fluids* **18** 053301
- [81] Korn C and Schwarz U 2006 Efficiency of initiating cell adhesion in hydrodynamic flow *Phys. Rev. Lett.* **97** 1–4
- [82] Gorba C and Helms V 2003 Diffusional dynamics of cytochrome c molecules in the presence of a charged surface *Soft Mater.* **1** 185–202
- [83] Korn C B, Klumpp S, Lipowsky R and Schwarz U S 2009 Stochastic simulations of cargo transport by processive molecular motors *J. Chem. Phys.* **131** 245107
- [84] Liron N and Shahar R 1978 Stokes flow due to a Stokeslet in a pipe *J. Fluid Mech.* **86** 727–44
- [85] Maul C and Kim S 1994 Image systems for a Stokeslet inside a rigid spherical container *J. Fluid Mech.* **6** 2221–3
- [86] Wojciechowski M, Szymczak P and Cieplak M 2010 The influence of hydrodynamic interactions on protein dynamics in confined and crowded spaces—assessment in simple models *Phys. Biol.* **7** 046011
- [87] Dingley A J, Mackay J P, Shaw G L, Hambly B D and King G F 1997 Measuring macromolecular diffusion using heteronuclear multiple-quantum pulsed-field-gradient NMR *J. Biomol. NMR* **10** 1–8
- [88] Garcia de la Torre J and Bloomfield V A 1981 Hydrodynamic properties of complex, rigid, biological macromolecules: theory and applications *Q. Rev. Biophys.* **14** 81–139
- [89] Antosiewicz J and Porschke D 1989 Volume correction for bead model simulations of rotational friction coefficients of macromolecules *J. Phys. Chem.* **93** 5301–5
- [90] Hellweg T, Eimer W, Krahn E, Schneider K and Müller A 1997 Hydrodynamic properties of nitrogenase—the MoFe protein from *azotobacter vinelandii* studied by dynamic light scattering and hydrodynamic modelling *Biochim. Biophys. Acta* **1337** 311–8
- [91] García De La Torre J, Huertas M L and Carrasco B 2000 Calculation of hydrodynamic properties of globular proteins from their atomic-level structure *Biophys. J.* **78** 719–30
- [92] Banachowicz E, Gapinski J and Patkowski A 2000 Solution structure of biopolymers: a new method of constructing a bead model *Biophys. J.* **78** 70–8

- [93] Banavar J R, Cieplak M, Hoang T X and Maritan A 2009 First-principles design of nanomachines *Proc. Natl Acad. Sci. USA* **106** 6900–3
- [94] Ripoll M 2006 Mesoscale hydrodynamics simulations *Computational Condensed Matter Physics* vol B5:1, ed S Blügel, G Gompper, E Koch, H Müller-Krumbhaar, R Spatschek and R G Winkler (Jülich: Forschungszentrum)
- [95] Noguchi H, Kikuchi N and Gompper G 2007 Particle-based mesoscale hydrodynamic techniques *Eur. Phys. Lett.* **78** 10005
- [96] Dünweg B and Ladd A J C 2009 Lattice Boltzmann simulations of soft matter systems *Advanced Computer Simulation Approaches for Soft Matter Sciences III (Advances in Polymer Science* vol 221) pp 89–166
- [97] Usta O B, Butler J E and Ladd A J C 2007 Transverse migration of a confined polymer driven by an external force *Phys. Rev. Lett.* **98** 098301
- [98] Izmitli A, Schwartz D C, Graham M D and de Pablo J J 2008 The effect of hydrodynamic interactions on the dynamics of DNA translocation through pores *J. Chem. Phys.* **128** 085102
- [99] Zhang Y, Donev A, Weisgraber T, Alder B J, Graham M D and de Pablo J J 2009 Tethered DNA dynamics in shear flow *J. Chem. Phys.* **130** 234902
- [100] Lemak A S and Balabaev N K 1996 Molecular dynamics simulation of a polymer chain in solution by collisional dynamics method *J. Comput. Chem.* **17** 1685–95
- [101] Brochard-Wyart F 1993 Deformations of one tethered chain in strong flows *Europhys. Lett.* **23** 105
- [102] Brochard-Wyart F, Hervet H and Pincus P 1994 Unwinding of polymer chains under forces or flows *Europhys. Lett.* **26** 511
- [103] Brochard-Wyart F 1995 Polymer chains under strong flows: stems and flowers *Europhys. Lett.* **30** 387–92
- [104] Lumley J 1969 Drag reduction by additives *Annu. Rev. Fluid Mech.* **1** 367–84
- [105] de Gennes P G 1974 Coil-stretch transition of dilute flexible polymers under ultrahigh velocity gradients *J. Chem. Phys.* **60** 5030–42
- [106] Smith D E, Babcock H P and Chu S 1999 Single-polymer dynamics in steady shear flow *Science* **283** 1724–7
- [107] Doyle P S, Ladoux B and Viovy J-L 2000 Dynamics of a tethered polymer in shear flow *Phys. Rev. Lett.* **84** 4769–72
- [108] Teixeira R E, Babcock H P, Shaqfeh E S G and Chu S 2005 Shear thinning and tumbling dynamics of single polymers in the flow-gradient plane *Macromolecules* **38** 581–92
- [109] Schroeder C M, Teixeira R E, Shaqfeh E S and Chu S 2005 Characteristic periodic motion of polymers in shear flow *Phys. Rev. Lett.* **95** 018301
- [110] Kobayashi H and Yamamoto R 2010 Tumbling motion of a single chain in shear flow: a crossover from Brownian to non-Brownian behavior *Phys. Rev. E* **81** 041807
- [111] Alexander-Katz A and Netz R 2008 Dynamics and instabilities of collapsed polymers in shear flow *Macromolecules* **41** 3363–74
- [112] Sing C E and Alexander-Katz A 2010 Globule-stretch transitions of collapsed polymers in elongational flow fields *Macromolecules* **43** 3532–41
- [113] Batchelor G K 1967 *An Introduction to Fluid Mechanics* (Cambridge: Cambridge University Press)
- [114] Henyey F S and Rabin Y 1985 Rotational isomeric model of the coil stretching transition of semiflexible polymers in elongational flow *J. Chem. Phys.* **82** 4362
- [115] de Gennes P G 1979 *Scaling Concepts in Polymer Physics* (Ithaca, NY: Cornell University Press)
- [116] Larson R G and Magda J J 1989 Coil-stretch transitions in mixed shear and extensional flows of dilute polymer solutions *Macromolecules* **22** 3004–10
- [117] Hernandez-Ortiz J P, Underhill P T and Graham M D 2009 Dynamics of confined suspensions of swimming particles *J. Phys.: Condens. Matter* **21** 204107
- [118] Drescher K, Leptos K, Tuval I, Ishikawa T, Pedley T and Goldstein R 2009 Dancing Volvox: hydrodynamic bound states of swimming algae *Phys. Rev. Lett.* **102** 1–4
- [119] Ekiel-Jezewska M L, Gubiec T and Szymczak P 2008 Stokesian dynamics of close particles *Phys. Fluids* **20** 1–10
- [120] Dickinson E 1985 Brownian dynamics with hydrodynamic interactions: the application to protein diffusional problems *Chem. Soc. Rev.* **14** 421–55
- [121] Tanaka H 2005 Roles of hydrodynamic interactions in structure formation of soft matter: protein folding as an example *J. Phys.: Condens. Matter* **17** S2795
- [122] Pitard E 1999 Influence of hydrodynamics on the dynamics of a homopolymer *Eur. Phys. J. B* **7** 665–73
- [123] Pham T T, Bajaj M and Prakash J R 2008 Brownian dynamics simulation of polymer collapse in a poor solvent: influence of implicit hydrodynamic interactions *Soft Matter* **4** 1196
- [124] Rzehak R, Kromen W, Kawakatsu T and Zimmermann W 2000 Deformation of a tethered polymer in uniform flow *Eur. Phys. J. E* **2** 3–30
- [125] Bagci Z, Jernigan R L and Bahar I 2002 Residue packing in proteins: uniform distribution on a coarse-grained scale *J. Chem. Phys.* **116** 2269